REDUCED ORDER MODELS FOR AERODYNAMIC APPLICATIONS, LOADS AND MDO

M. J. Verveld[*] · **T. M. Kier**[*] · **N. W. Karcher**[†] · **T. Franz**[†] · **M. Abu-Zurayk**[†] · **M. Ripepi**[†] · **S. Görtz**[†]

Abstract

This work gives an overview of reduced order model (ROM) applications employed within the context of the DLR Digital-X project. The ROM methodology has found widespread application in fluid dynamics. In its direct application to computational fluid dynamics (CFD) it seeks to reduce the computational complexity of a problem by reducing the number of degrees of freedom rather than simplifying the physical model. Here, parametric aerodynamic ROMs are used to provide pressure distributions based on high-fidelity CFD, but at lower evaluation time and storage than the original CFD model. ROMs for steady aerodynamic applications are presented. We consider ROMs combining proper orthogonal decomposition (POD) and Isomap, which is a manifold learning method, with interpolation methods as well as physics-based ROMs, where an approximate solution is found in the POD-subspace or non-linear manifold by minimizing the corresponding steady or unsteady flow-solver residual. The issue of how to train the ROM with high-fidelity CFD data is also addressed. The steady ROMs are used to predict the static aeroelastic loads in a multidisciplinary design and optimization (MDO) context, where the structural model is to be sized for the (aerodynamic) loads. They are also used in a process where an a priori identification of the critical load cases is of interest and the sheer number of load cases to be considered does not lend itself to high-fidelity CFD. We also show an approach combining correction of a linear loads analysis model using steady, rigid CFD solutions at various Mach numbers and angles of attack with a ROM of the corrected Aerodynamic Influence Coefficients (AICs). This integrates the results into a complete loads analysis model preserving aerodynamic nonlinearities while allowing fast evaluation across all model parameters. Thus, correction for the major nonlinearities, e.g. depending on Mach number and angle of attack combines with the linearity of the baseline model to yield a large domain of validity across all flow parameters at the expense of a relatively small number of CFD solutions. The different ROM methods are applied to a 3D test case of a transonic wing-body transport aircraft configuration.

Keywords reduced order model · proper orthogonal decomposition · manifold learning · multidisciplinary design and optimization · aerodynamic influence coefficients · loads analysis

1 Introduction

The multidisciplinary design of a civil transport aircraft is a highly iterative optimization process, each design cycle requiring a large volume of computations to analyse the current performance, handling qualities and loads. E.g., a loads envelope may require on the order of 100.000 simulations to find all critical loadcases. These analyses typically cover large parts of the flight envelope and may require high fidelity aerodynamic data, i.e. steady and unsteady pressure and shear stress distributions on the aircraft surface, at any point within this envelope. The advent and development of large-scale high-fidelity computational fluid dynamics (CFD) in aircraft design increasingly

requires procedures and techniques aimed at reducing its computational cost and complexity in order to provide accurate but fast simulations of, e.g., the aerodynamic loads and performances.

A classical approach to reduce the numerical complexity involved with these aircraft design problems would be to simplify the physics modeling involved to make analysis manageable. An example of this is the common use of linear potential flow equations during loads analysis. However, such physical model simplifications have the disadvantage of neglecting significant effects such as transonic flow, stall and friction drag in the case of aerodynamics. This may be acceptable early on in the design process, where more detailed analysis may be applied at a later stage when the design space has been narrowed down sufficiently. As an alternative to simplifying the physics model, reduced order modeling (ROM) provides another ap-

[*]DLR - German Aerospace Center, Institute of System Dynamics and Control, 82234 Wessling, Germany

[†]DLR - German Aerospace Center, Institute of Aerodynamics and Flow Technology, 38108 Braunschweig, Germany

proach to reduce numerical complexity. The various ROM methods do this in general by exploiting similarity within an ensemble of high fidelity "snapshot" solutions which sample a certain parametric domain of interest. The number of degrees of freedom (DoF) is then reduced while retaining the problem's physical fidelity, thus allowing predictions of the aerodynamic data to be provided with lower evaluation time and storage than the original CFD model.

This paper reports on ROM methods developed and employed within the context of the Digital-X project. Digital-X is a DLR-project focusing on the development of numerical simulation methods for the design of aircraft. The primary objective of the project is the development of a software platform for multidisciplinary design and optimization (MDO) of aircraft and helicopters based on high-fidelity numerical methods. The global Digital-X MDO process chain is shown in Fig. 1. It is a collaborative effort including aerodynamics, structure, mass estimation, engine and flight performance, control and other disciplines contributed by several DLR institutes [18]. The MDO chain iterates through three successive detail levels: the preliminary design level, the dynamic level responsible for loads analysis and initial structure sizing and the detailed level where performance is optimized through high fidelity analysis methods. These are controlled by a global optimizer and use Common Parametric Aircraft Configuration Schema (CPACS) as a design data exchange format [43].

Several methods have been employed to obtain reduced order models (ROMs) for the prediction of steady and unsteady aerodynamic flows using low-dimensional linear subspaces [44, 45, 39, 46] as well as nonlinear manifolds [16], whose performances may be further improved [40, 47] by applying sampling techniques and hyper-reduction procedures (e.g. empirical interpolation method [5, 11] and missing point estimation [2, 3]). These techniques and methods are implemented in the DLR's SMARTy toolbox.

The Airbus XRF-1 transport aircraft configuration is used as the reference geometry in the following to demonstrate the capabilities of the different MDO approaches. The XRF-1 is a generic research configuration similar to an existing Airbus wide-body aircraft. Figure 2 shows the baseline XRF-1 geometry, which is a wing/fuselage/tail configuration. It was specified consistently in CPACS format including a simplified 8,000 nm mission consisting of climb, cruise, descent and landing as well as a flight to an alternate airport (200 nm). As no payload-range diagram and Top-
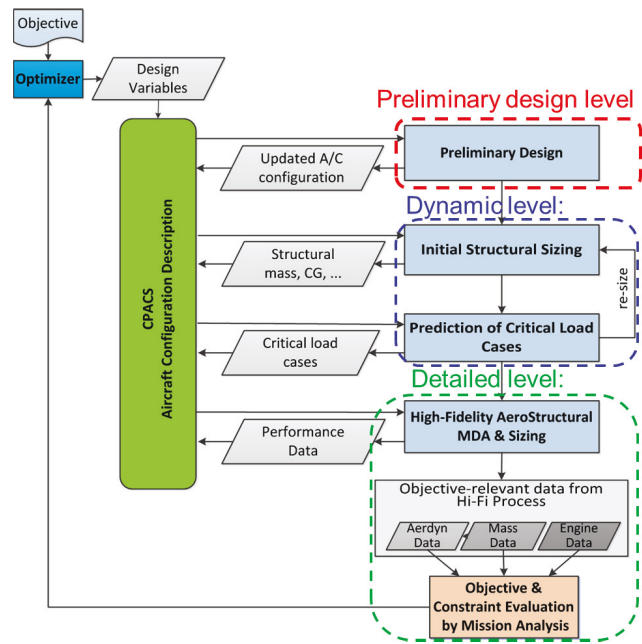

Fig. 1 The Multidisciplinary Design Optimization Process Chain as used in the Digital-X project [22]
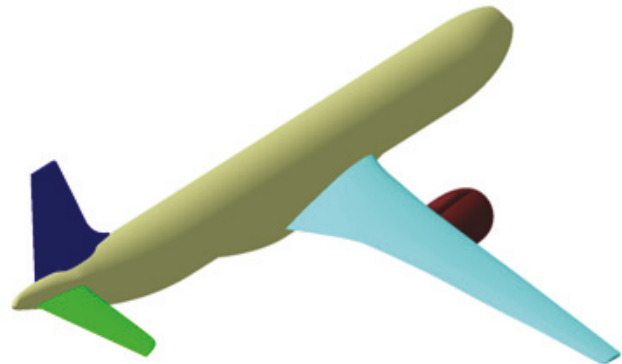

Fig. 2 XRF-1 generic long-range transport aircraft used as a baseline for MDO

Level Aircraft Requirements (TLARs) were available for the XRF-1, they were reconstructed with the help of DLR's preliminary design tools. Adjustments were done where necessary to create a consistent data set. A selection of the reconstructed TLARs is given in Table 1. The TLAR were validated by performing a simulation of the reference long-range mission with the preliminary design tools, showing good agreement with Airbus reference data for this mission.

The paper is organized as follows. Section 2 gives a general description of ROM methods. Then section 3 describes methods which are part of the "High-Fidelity AeroStructural MDA & Sizing" process in

Table 1 Reconstructed TLAR (selection)

TLAR	Value
Design range [nm]	5600
Max. range @ MTOW [nm]	≥ 8000
Cruise alt [ft]	35000
Cruise Mach number	0.83
PAX #	353
Max. payload [10^3 kg]	≥ 48
Max. take-off thrust/engine [kN]	334.7
Take-off field length	≤ 2700 m

Fig. 1. In this context the goal is to build a parametric ROM providing a prediction of static aeroelastic loads over the design space of the possible wing aerodynamic shapes, wing-box structural properties, and design load cases. Given the inherent difficulty (due to the high number of parameters and the strong interaction between coupled disciplines) in building such a global ROM, we use a divide-and-conquer strategy where ROMs are built separately for different subproblems.

Section 4 describes an application of a ROM for the loads analysis and sizing process comprizing the dynamic level in Fig. 1. Here, Proper Orthogonal Decomposition (POD) has been applied to CFD corrected steady Aerodynamic Influence Coefficient (AIC) matrices and coupled to Thin Plate Spline (TPS) interpolation to create a ROM of corrected AICs for loads analysis. This bridges the gap between CFD based methods and classical loads analysis. The AIC-ROM provides a parameter-complete aeromodel, as required for loads analysis, regardless of the dimensionality of the snapshot parameterspace used for correction. The AIC-ROM has been implemented to work with VarLoads [19], a Loads Analysis tool developed jointly by DLR and Airbus.

2 Reduced-Order Modeling

Reduced-order models for aerodynamic applications operate on parametrically generated data, the so called *snapshots*, represented by either surface quantities (e.g. surface pressure and shear stress) or volume quantities (e.g. the primitive variables). The DLR TAU code [35, 23] is utilized as CFD solver, employing hybrid unstructured grids, to obtain the aerodynamic data snapshots. The parameters can be related to the flow (e.g. the angle of attack, the Mach number), the geometry (e.g. wing span, taper ratio, and sweep angle), the

structure (e.g. Young's and shear modulus of the beam representation of the wing box) and the flight condition (e.g. load factor, altitude).

The model order reduction techniques used within the DLR Digital-X project are hereafter briefly described, and their application within the MDO framework for loads prediction, critical loads cases selection, structural sizing and correction of low-fidelity aerodynamic methods is shown in the following sections.

2.1 POD-based ROM

A widely used tool is proper orthogonal decomposition (POD) [20, 38, 34], also known as principal component analysis (PCA) [36] and Karhunen Loéve expansion. POD is well established and used in diverse fields such as image processing, signal analysis, data compression, process identification and control in chemical engineering [24]. In fluid dynamics, it is applied to steady problems and unsteady problems in the time as well as frequency domain. The POD method generates a sequence of orthogonal basis functions through modal analysis of an ensemble of snapshot flow solutions, which span an optimal linear subspace for the corresponding solution space. By choosing a subset of modes the method seeks to isolate the few main structures whose linear combination represents the system in an optimal way.

Several variants of POD based methods have been developed which primarily differ in the way how they connect the retained modes to the parameter space of the snapshot distribution. The POD may be embedded in a Galerkin projection framework [26, Sect. 2.2.4], it may be combined with a CFD flux residual minimization scheme [24, 45], or it may be coupled to an interpolation method (POD+I) [9, 14].

These POD methods may be cathegorized as either intrusive or non-intrusive [13]. Galerkin projection is an example of an intrusive method. It projects the underlying spatially discretized partial differential equations (PDEs) onto the POD subspace to obtain a system of ordinary differential equations (ODEs). Within the DLR Digital-X project, the ROM predicted solution is conversely determined by directly computing the coefficients of the POD modes, without the need to solve the ODE system. We do this through interpolation, referred to as *POD+I*. This is a non-intrusive method as the interpolation technique does not require any details on the underlying governing equations. It generally establishes a multi-dimensional relationship between the modal coefficients or amplitudes and the

parameter space, e.g. by fitting a radial basis function network in the modal space to the set of snapshot points in the parameter space. This has the advantage of simplicity of implementation and independence of the complexity of the system and source of the modes being processed, which allows for application to multidisciplinary problems and the combination of different data sources such as CFD and experimental test results.

The main disadvantage of non-intrusive POD methods stems from their reliance on interpolation techniques to accurately reproduce the possibly very nonlinear response surfaces of the modal coefficients. Intrusive POD methods do better in this respect. Within the DLR Digital-X project, we do this through an optimization problem which minimizes the residual of the underlying equations, which will be referred to as *POD+LSQ*.

2.2 Isomap-based ROM

The linear nature of the POD makes the method attractive but also is the source of its restriction. Highly non-linear flow phenomena, such as shocks, are often insufficiently reproduced, because of the underlying assumption that the full-order CFD flow solution lie in a low-dimensional linear subspace. An approach to improve the fidelity of linear ROMs is to subtitute the POD with a nonlinear manifold learning (ML) [10, 27, 30, 7], or, more generally, dimensionality reduction (DR) technique. This shifts the burden of reproducing complex flow phenomena from the interpolation to the DR technique, by assuming that full-order data lies on a nonlinear manifold of low-dimension. Such techniques try to solve the so-called embedding problem. In general, this is an ill-posed problem, because neither the geometry of the data nor the intrinsic dimensionality is known.

Within the DLR Digital-X project, the Isomap [37] method, which is a nonlinear DR method based on multi-dimensional scaling (MDS) [28], is employed to extract low-dimensional structures hidden in a given high-dimensional data set.

The Isomap method only provides a mapping from the high-dimensional input space onto a lower-dimensional embedding space for a fixed finite set of given snapshots. For any ROM of the Navier-Stokes equations, however, it is an essential requirement that the approximate reduced-order flow solutions are of the same type and dimension as the full-order CFD snapshots. Hence, once the set of low-dimensional vectors is obtained, a back-mapping from the reduced-order embedding to the high-dimensional solution space is mandatory.

Coupled with an interpolation model formulated between the parameter space and the low-dimensional space, a ROM is obtained which is capable of predicting full-order solutions at untried parameter combinations. This method will be referred to as *Isomap+I*.

Furthermore, another back-mapping from the low-dimensional space to the high-dimensional space may be performed based on the residual optimization. Its objective is to obtain a CFD-enhanced prediction by minimizing the discretized flux residual of the interpolated solution. This method will be referred to as *Isomap+LSQ*.

3 Reduced-Order Models for Static Aeroelastic Loads

In this section we present a reduced order modeling process for computing static aeroelastic loads, to be used in the framework of high-fidelity MDO [32] and sizing process as shown in Fig. 3. The method consists of building a ROM from static aeroelastic solutions computed for different sets of parameters. Such solutions are collected in a snapshot matrix, to which a POD [9] or an Isomap [37] embedding is applied in order to get a (linear or nonlinear) low-dimensional subspace. A reduced order model, either POD-based or Isomap-based, is built from static aeroelastic solutions computed for different sets of parameters like, e.g., flight conditions (altitude, number of Mach, load factor), flight configurations (payload mass, fuel mass), geometrical parameters (wing planform parameters as aspect ratio, taper ratio, swept angle, and the twist angle for selected airfoil sections) and structural properties (wing-box stiffness and mass). The parameter space is sampled using Design of Experiment (DoE) techniques [12].

However, the integrated nature of the MDO process involves complex interactions between the different disciplines, which are difficult to be represented with a single global ROM, if not at the expense of a costly sampling of the whole paramater design space with multidisciplinary high-fidelity simulations. Being understood that such a global ROM may be devised and sought in future works and projects, hereafter an efficient approach to manage this complexity is shown, where a divide-and-conquer strategy is applyed and the MDO is decomposed in sub-processes, for which small parametric ROMs can be easier generated separately and used for fast system-level analysis.

First, section 3.1 describes how to construct a ROM of coupled, static aeroelastic solutions for a given (flex-
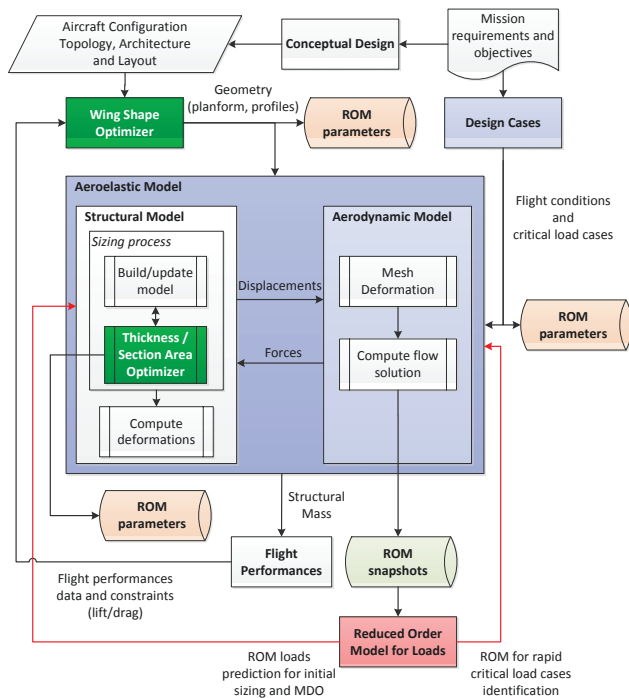
Fig. 3 Flow chart of the reduced order modelling for loads in the MDO framework.

Fig. 4 Detailed view of the surface of the CFD structured grid of the XRF-1 configuration.

Fig. 5 Structural finite element model of the wing, showing the front, rear and middle spars, and the ribs.

ible) aero-structural configuration and different load cases (in Fig. 3, ROM of the *Aeroelastic Model* block, w/o *Sizing Process*, and parameters the *flight conditions*). Then section 3.2 describes how to select critical load cases based on an aeroelastic ROM built for a given aerodynamic shape, but structure sized over different load cases (in Fig. 3, ROM of the *Aeroelastic Model* block, with *Sizing Process*, and parameters the *load cases*). Section 3.3 shows a ROM for steady aerodynamic loads predictions of a rigid XRF-1 configuration subject to geometry variations (in Fig. 3, ROM of the *Aerodynamic Model* block and parameters the *Geometry*), which is afterwards used (section 3.4), for a given aerodynamic shape and load case, in the structural sizing sub-process.

3.1 Static Aeroelastic Loads of the XRF-1 Aircraft

Here are presented the performances and effectiveness of the ROM approach in predicting static aeroelastic loads for the three-dimensional XRF-1 fuselage-wing configuration in the transonic flow regime.

The geometry of the configuration and the underlying structured grid featuring 784,384 grid points, including 19,211 surface grid points, are depicted in Fig. 4. The aerodynamic model is a Reynolds-Averaged
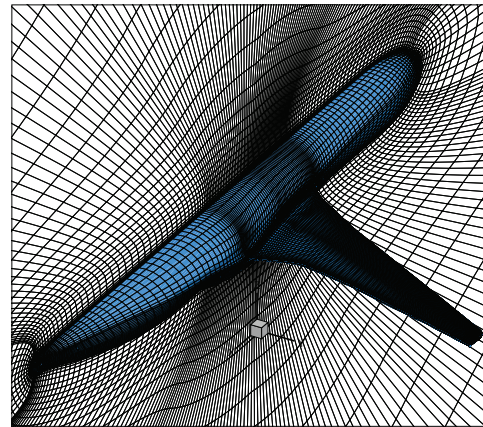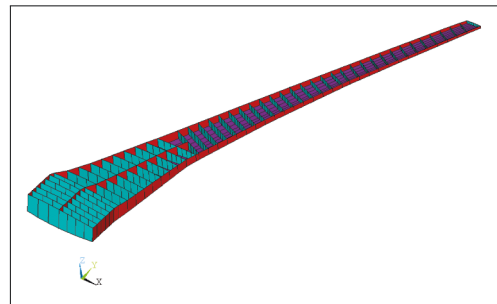
Navier-Stokes (RANS) model with a negative Spalart-Allmaras type 1-equation turbulence model [1] and solved using the computational fluid-dynamics (CFD) DLR TAU solver [35, 23]. Whereas the computational structural model (CSM) is spatially discretized by using finite element shells and beams with 2167 elements (1914 shells, 212 beams and 41 mass type elements) and 1725 nodes, as showed in Fig. 5. The ANSYS Structural Mechanics software is used for the finite element analysis. The coupling between the aerodynamic and the structural model is obtained through the use of Radial Basis Functions (RBFs) [6] to transfer the aerodynamic loads to the structural model, and a linear interpolation of the structural displacements onto the aerodynamic grid.

The aircraft empty mass is 117888.2 kg. A flight configuration with 55000 kg of payload mass and 61000 kg of fuel mass is considered. Pull-up and pull-down maneuvers, of respectively load factor 2.5 g and -1 g, are analyzed.

The computation of the coupled flow-structure solutions were performed in parallel on the DLR $C^2A^2S^2E$-2 cluster using 2 nodes[1] with 24 cores. Computing a free-flight coupled CFD (TAU) - CSM (ANSYS) static aeroelastic solution took an average[2] of 2430 wall-clock seconds.

The aeroelastic equilibrium and the trim correction[3] are computed independently with two nested loop. Each iteration to find the static aeroelastic equilibrium (outer loop) involves interpolation of the displacements from the CSM to the CFD mesh, deformation of the CFD mesh using RBFs, computation of the flow solution (with inner loop target C_L trimming strategy), interpolation of the forces from the CFD model to the CSM mesh, and computation of the structure solution.

An average of 4 coupling outer iterations are necessary for the static aeroelastic convergence. In each of these coupled iterations, the solution of the trim is obained through a target C_L strategy, where the angle of attack is determined so as to provide a lift balancing the aircraft weight and the inertial force due to a given load factor. Here the CFD subsystem is solved by first using a minimum iteration strategy, running 3500 iterations, followed by a minimum residual strategy, where the density residual is converged by four orders of magnitude at the initial coupled iteration, up to six orders of magnitude proceeding with the coupled iterations. In the minimum residual strategy a maximal inner iteration number of 9950 is anyhow set-up.

For the test case presented, the ROM is parametrized only upon flight conditions, i.e., altitude and Mach number. Choosing suitable flight conditions and configurations parameter combinations for the snapshot computation is a very important issue in building the ROM. In this case, static aeroelastic high-fidelity simulations have been performed (offline) for a Mach number ranging from 0.65 to 0.82, and an altitude between 0 m and 5000 m. The payload and fuel masses are kept fixed. The sample points are computed using a full factorial design strategy over the Mach number

---

[1]Intel® Xeon® E5-2695 v2 Processors (30M Cache, 2.40 GHz, 12 Cores)

[2]Based on the effectively computed reference solutions, i.e. without taking into account the not converged simulations.

[3]It must be noted that the aircraft model is missing the horizontal tail plane (HTP). Therefore, the equilibrium condition is applied only in the vertical translation direction. The aircraft pitching moment will not be trimmed, and the resulting wing lift will therefore only balance the inertial loads and not the (usual) negative lift of the HTP. Despite only the vertical equilibrium is considered, the coupled procedure still offers fluid-structure snapshots suitable to verify the soundness of the ROM capability in predicting approximate solutions.
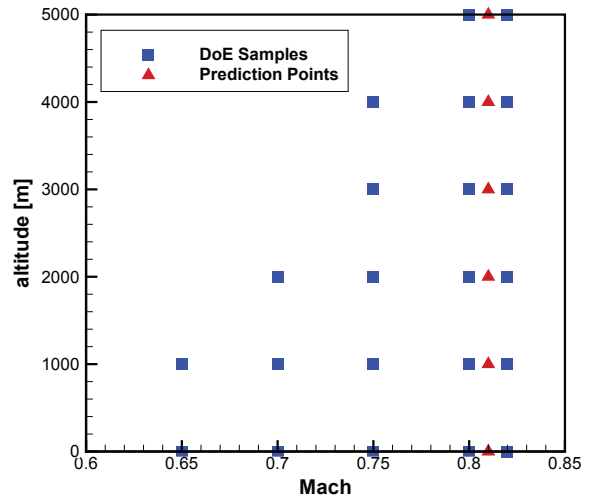

Fig. 6 Design of experiment samples and prediction points.

range between 0.65 and 0.80, with additional points along Mach 0.82. Only the converged solutions, i.e. 22 snapshots, have been taken into account in the ROM generation procedure. The ROM is realized through a POD of the high-fidelity snapshots together with a Thin Plate Spline (TPS) method interpolating the POD coefficients to get the predicted aeroelastic solution (i.e. the surface pressure, the skin friction and the structural displacement). All the POD modes have been reteined. The performances of the ROM approach are evaluated at flight conditions with Mach number 0.81, for different altitudes. The prediction points and the DoE sample points are shown in Fig. 6.

Before computing the ROM predictions, a leave-1-out cross-validation strategy has been performed to understand if the set of sample points were enough to cover the parameter space. Therefore, following this strategy, alternately one of the high-fidelity snapshots of the DoE sample set has been left out from the ROM generation procedure (which is then built using the remaining 21 DoE sample snapshots as the training set, retaining all the 21 POD modes). In the corresponding flight condition of the left-out snapshot (i.e. the validation point) the ROM prediction has been performed. This prediction has been compared to the high-fidelity computation in terms of aerodynamic coefficients.

It must be noted that the inputs of the reduced order model are only the Mach number and the altitude. Therefore the ROM aeroelastic prediction is not associated with any angle of attack. The only information about the freestream boundary condition is related to
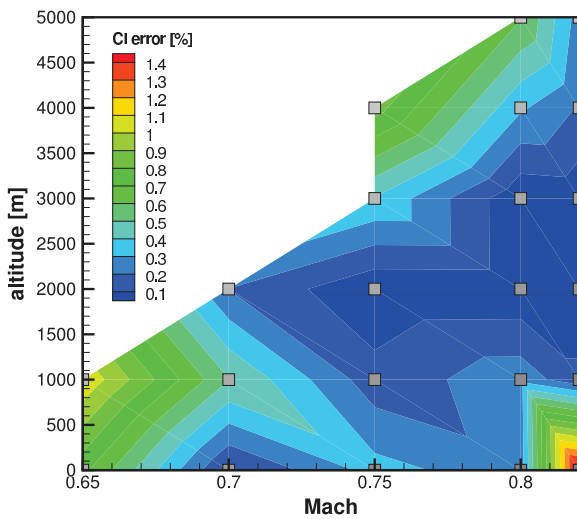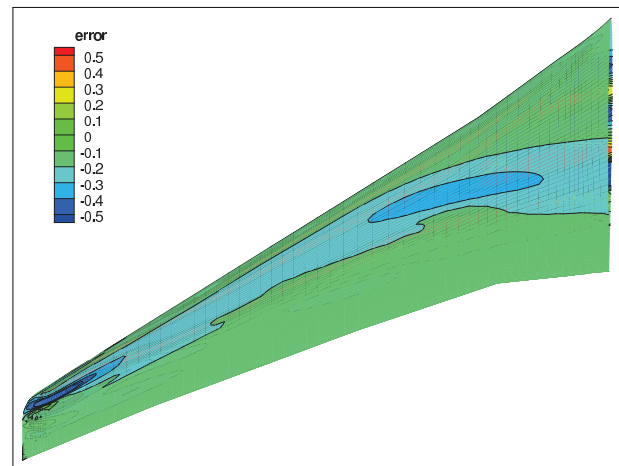
Fig. 7 Relative error, between the HFM and the ROM prediction, of the lift coefficient to trim the aircraft.

the airspeed absolute value (i.e. the Mach number). This is because the coupled CFD/CSM static aeroelastic solutions have been obtained through a trim procedure using a *target C_L* strategy, i.e. the lift coefficient is an input of the procedure, and the angle of attack (together with the aerodynamic forces, for the given deformed structure) is an output. Therefore, in order to have a comparison in terms of aerodynamic coefficients with the high-fidelity static aeroelastic solution, a proper angle of attack must be selected. Here, the same angle of attack resulting from the high-fidelity trimming procedure is used.

Figure 7 shows the error between the lift coefficient computed with the coupled TAU/ANSYS high-fidelity model (HFM), necessary to (vertically) trim the aircraft in the various flight conditions, and those predicted by the reduced order model. A linear interpolation is used to compute the C_L between flight condition sample points. Generally, the error is greater in those prediction points outside of the convex hull of the training set under consideration, where the ROM prediction consists of an extrapolation. It must be noted that the ROM predictions in the such validation points may be quite challenging. Indeed, for each validation point the nearby high-fidelity solutions used as training set to build the ROM are distant ±0.5 in terms of Mach number and ±1000 m in terms of altitude.

As example, the relative error in percentage between the lower and upper pressure on the wing of the reference high-fidelity model and the ROM prediction, for the validation point $(h, Ma) = (1000\,\text{m}, 0.75)$

(a) Lower surface.
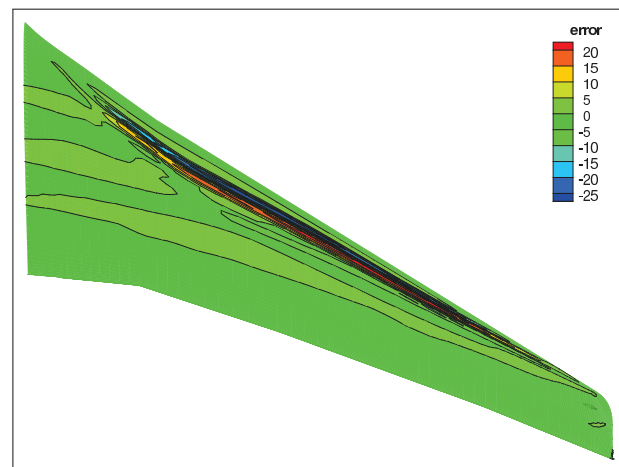
(b) Upper surface.

Fig. 8 Relative error, in percentage, of the wing pressure distribution between the high-fidelity and the ROM, in the validation point h = 1000 m, Ma = 0.75.

(and load factor 2.5 g) is shown in Fig. 8. The greater error is found in correspondence to the shock wave. A comparison of the structural displacements for such points can be seen in Fig. 9.

After the leave-1-out cross-validation, ROM predictions have been performed at Mach number 0.81. Results are summarized in Table 2. In this case, the relative error between the high-fidelity aeroelastic solution and the ROM prediction is very low, not greater than 0.1% for the lift coefficient and not greater than 0.35% for the drag coefficient. Figure 10 compares, for the case of 4000 m of altitude (and load factor 2.5 g), the surface pressure distributions predicted by the aeroelastic ROM with the reference coupled CFD–CSM solution. The pressure distribution is visualized on the aircraft jig shape in order to have better comparison of the results.
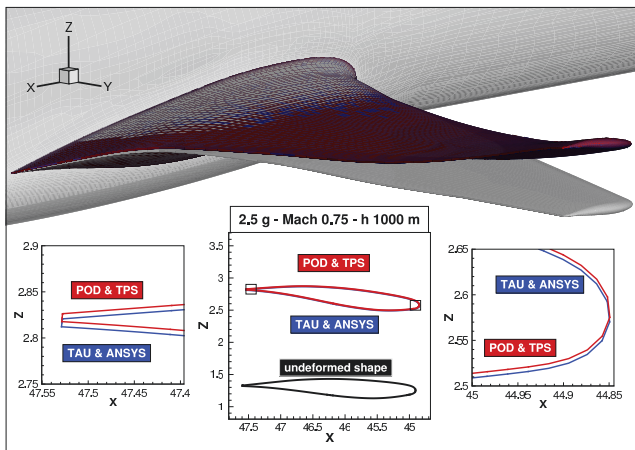
Fig. 9 Comparison of the wing structural displacement between the coupled high-fidelity model (TAU-ANSYS) and the reduced order model (POD-TPS), in the validation point h = 1000 m, Ma = 0.75, n = 2.5 g.

Table 2 Relative error between the aerodynamic coefficients of the trimmed high-fidelity aeroelastic model (HFM) and the corresponding ROM predictions using the Hi-Fi trimming angle of attack α.

		0	1000	2000	3000	4000	5000
	h [m]						
HFM	α [deg]	1.963	2.319	2.767	3.330	4.064	4.965
	C_L	0.370	0.417	0.472	0.535	0.608	0.694
	C_D	0.0229	0.0255	0.0294	0.0355	0.0452	0.0607
	C_{My}	-2.263	-2.545	-2.870	-3.248	-3.687	-4.200
ROM	C_L	0.370	0.417	0.472	0.535	0.608	0.694
	C_D	0.0228	0.0254	0.0294	0.0354	0.0453	0.0608
	C_{My}	-2.265	-2.545	-2.872	-3.248	-3.686	-4.202
Err. [%]	C_L	0.091	0.043	0.035	0.013	0.011	0.035
	C_D	0.130	0.319	0.008	0.093	0.087	0.253
	C_{My}	0.084	0.000	0.050	0.010	0.008	0.038

The ROM prediction is obtained in 78 seconds, in sequential mode, including the data processing (e.g. loading the snapshots from memory) and building the ROM (i.e. the POD modes generation), where only 0.014 seconds are demanded for the online prediction of the aeroelastic solution (in terms of surface pressure distribution and structural displacements). The achieved ROM speed-up factor for the wall-clock time is 31, when the offline ROM generation is also taken into account in the total ROM process wall-clock time. The speed-up rises up to 173571, when only the online prediction is considered. In these speed-up factors, the offline cost required to get the 21 high-fidelity coupled simulations is not considered.

3.1.1 Considerations and Remarks

The ROM shows a good prediction capability in terms of aeroelastic loads for multidisciplinary optimization and high-fidelity sizing.

The major discrepancies are near the shock wave. A better prediction could be achieved using the Isomap technique, which already showed to perform better than POD-based ROMs in predicting the shock position and intensity for steady aerodynamic computations [16]. Further, better results could be achieved with a different sampling strategy, e.g. a random Latin hypercube [12], more suitable for ROM generation, and using a larger number of samples.

Nevertheless these discrepancies, when the ROM is employed within the MDO process, it would not affect the result of the optimization in terms of final design, as will be shown for the sizing process in Section 3.4.

As final remark, a different physical modelling (e.g. unsteady RANS or Hybrid RANS/LES) would be necessary in those sample points of the flight envelope where the aeroelastic solution is not converged, in order to properly model the unsteadiness of the separated flow and the effect of the time varying aerodynamic load on the structure and the aeroelastic trim.

3.2 Critical Load Case Selection through ROMs

Aiming to an aeroelastic structural optimization of the XRF1 aircraft able to withstand the critical loads, the Mach-altitude envelope for five critical mass cases has been computed, and the relative critical aerodynamic load cases have been determined. The five mass cases considered were the operating empty mass, two maximum take-off mass cases, once with maximum fuel and once with maximum payload, a mass case with zero payload and maximum fuel, and a mass case with zero fuel and maximum payload. The Mach-altitude envelope for the five mass cases was computed at intervals of 0.02 in Mach, and of $1000\,m$ in altitude for two load factors $(-1g, 2.5g)$.

After computing the aerodynamic load envelope of the flexible aircraft (i.e. the aerodynamic pressure distribution of the static aeroelastic solution), all the loads were given in input to the sizing tool S-BOT. This tool provides as an output to the designer the critical loads and the relative sized structure able to sustain such loads. By modifying the structure, the process needs to be iterated re-computing the aerodynamic loads until convergence.

Since this process is very computationally expensive, POD-based ROMs were employed using the DLR's SMARTy toolbox. Here ROMs were used to explore the
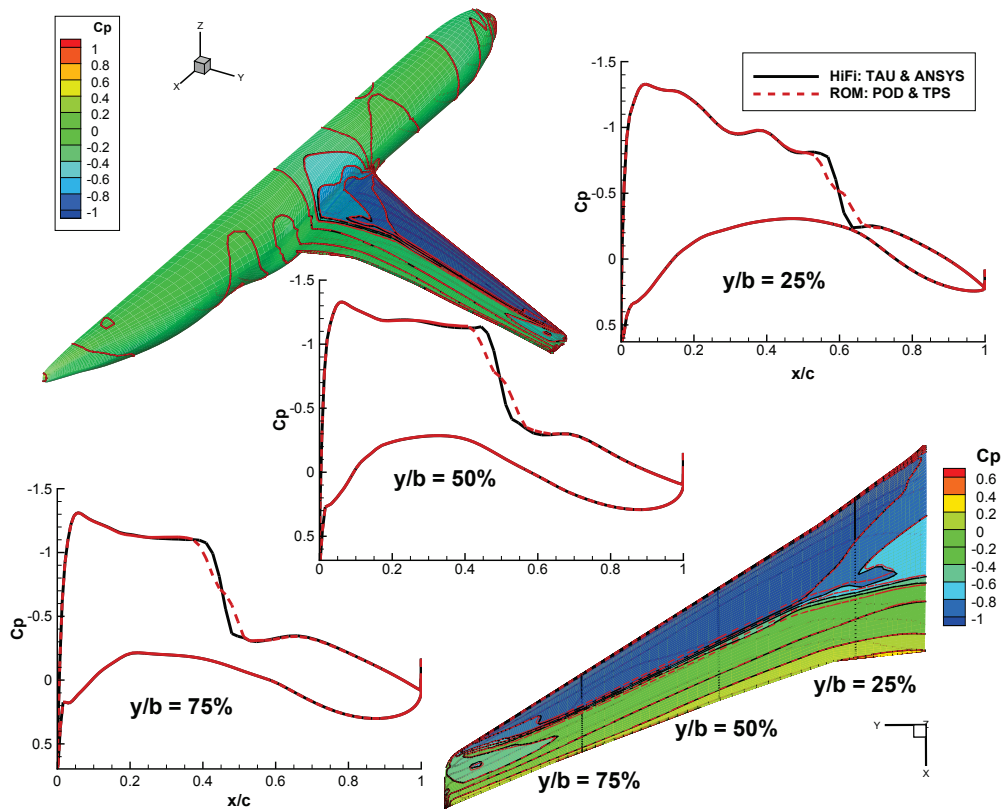
Fig. 10 Comparison of the pressure distribution at the 25%, 50% and 70% spanwise airfoil sections, for Mach 0.81 and altitude 4000 m.

parameter space with a finer sampling at in-between altitudes. The (in-between altitudes) ROM predicted aeroelastic loads are sent to the sizing tool, which determines if the loads are critical. Whenever a newly predicted aeroelastic load is found to be potentially critical, the corresponding load case is recomputed with the high-fidelity coupled CFD-CSM methods and checked with the sizing tool if it is really critical or not.

As an example, two of the five critical mass cases were used to generate 400 sized high-fidelity aeroelastic snapshots. A parametric reduced-order model has been generated using such snapshots, and then used to compute 360 additional loads predictions. Of these 360 predictions, 3 were found to be additional candidates for critical load cases, and by computing them with the high-fidelity tools one case was found to be actually critical. Figure 11 shows the complete aerodynamic load case identification process.

This process guarantees an efficient search and selection for new critical load cases. However, it should be pointed out that the prediction capability of the ROMs depends on the high fidelity snapshots used to generate them. Reduced-order models after all are
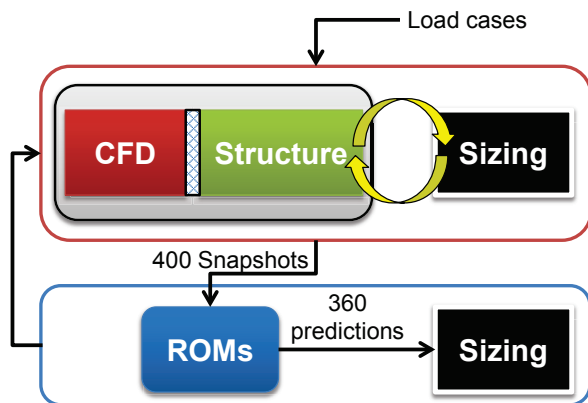

Fig. 11 The load case identification process.

nothing else than a linear combination of the approximation of such snapshots. Therefore it may possible that the ROMs can fail to provide additional candidates for the critical load cases, which might turn out to be critical for the sizing process if computed with high-fidelity methods.
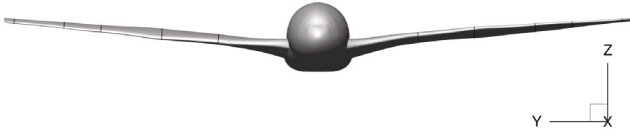
Fig. 12 Front view of the XRF-1. Twists are performed at five section cuts depicted by the black lines on the wing. The left and the right wing show the maximum twists in different rotation directions.

3.3 Parametric ROMs for Aero-Data in MDO

This section shows the use of parametric, Isomap-based, reduced-order models for the prediciton of the aerodynamic loads of the rigid XRF-1 aircraft, subject to wing geometry variations. The Mach number and the Reynolds number are here fixed respectively at $\mathrm{Ma} = 0.83$ and $\mathrm{Re} \approx 43.4 \cdot 10^6$. Furthermore, a target lift coefficient of $C_l = 0.5$ is prescribed. The twist of five wing sections are used as parameters of the ROM. The wing sections positions and the maximum twist in different rotation directions are shown in Fig. 12.

An adaptive sampling with a hybrid error (HYE) strategy [15] is employed to generate a sampling of the high-dimensional data manifold $\mathcal{W}$. The data manifold $\mathcal{W}$ is given by varying the five twist parameters of the configuration in the parameter space $\mathcal{P} = [-0.2, 0.2] \times [-2, 2] \times [-3, 3] \times [-2, 2] \times [-1, 1] \subset \mathbb{R}^5$, where the intervals from left to right correspond to the twist sections from fuselage to tip. A total of 100 viscous flow solution snapshots have been computed with the TAU RANS solver, whereby the normalized density residual is reduced by six orders of magnitude for each solution. Since a target lift coefficient of $C_l = 0.5$ is aimed at, the angle of attack α varies during the CFD simulation until the target lift is matched.

The sampling process including the computation of the flow solutions and all further computations were performed in parallel on the DLR $\mathrm{C^2A^2S^2E}$-2 cluster using one node endowed with 128 GB RAM and two Intel® Xeon® E5-2695 v2 Processors (30M Cache, 2.40 GHz, 12 Cores). Computing a full CFD solution for this test case took 5393 iterations or 4214 CPU seconds on average.

Once the data manifold $W = \{\mathbf{W}^1, \dots, \mathbf{W}^{100}\} \subset \mathcal{W}$ is obtained, with corresponding parameter set $P = \{\mathbf{p}^1, \dots, \mathbf{p}^{100}\} \subset \mathcal{P}$, the Isomap based ROMs predictions are computed at untried points $\tilde{\mathbf{p}} \in \mathcal{P} \setminus P$. Such points $\tilde{\mathbf{p}}$ were chosen as the centers of the 10 simplices with the largest volume of the *Delaunay tri-*

angulation [33, 4] of P, so as to maximize their distance from each $\mathbf{p} \in P$. The error at a prediction point $\mathbf{p} \in \mathcal{P}$ is computed as:

$$\mathrm{err}(\mathbf{W}^{\mathrm{ref}}(\mathbf{p}), \mathbf{W}^*(\mathbf{p})) = \frac{\sum_{i \in \mathcal{I}_R} |\mathbf{W}_i^{\mathrm{ref}} - \mathbf{W}_i^*|}{\sum_{i \in \mathcal{I}_R} |\mathbf{W}_i^{\mathrm{ref}}|} \qquad (1)$$

being $\mathbf{W}^{\mathrm{ref}}(\mathbf{p}) \in \mathbb{R}^n$ and $\mathbf{W}^*(\mathbf{p}) \in \mathbb{R}^n$ respectively the reference solution and the ROM-based prediction at $\mathbf{p} \in \mathcal{P}$, and n the product of the number of grid points and the number of variables, i. e. $n = n_g n_v$.

As will be shown, the results are accurate. Hence, the Isomap based ROMs for aero-data can be exploited for a multidisciplinary optimization within the whole parameter space, saving the costs of computing full-order CFD solutions.

3.3.1 Isomap with Interpolation

The interpolation based ROM makes use only of the surface snapshots, hence $\mathbf{W}^i \in \mathbb{R}^{19,211}$. Since five parameters are varied, the Isomap algorithm is applied to surface C_p-distribution vectors to compute a 5-dimensional embedding consisting of 100 representatives $\mathbf{y}^i \in \mathbb{R}^5$. The neighborhood graph is built using 87 nearest neighbors, and the back-mapping employes between $10 - 20$ nearest neighbors.

For comparison purposes, a global POD of the 100 full-order surface C_p snapshots is performed, yielding a basis consisting of 99 orthonormal POD eigenmode vectors[4] of dimension 19,211. As before, the POD model is combined with a TPS interpolation scheme [15, 6]. Compared to Isomap+I, where a representative $\mathbf{y}^* \in \mathbb{R}^5$ of dimension five has to be interpolated to obtain a surface C_p prediction, POD+I employs TPS to interpolate the POD coefficient vector $\mathbf{a} \in \mathbb{R}^{99}$ of much larger dimension.

Isomap+I and POD+I were built in 119 and 0.17 CPU seconds, respectively, including the data processing, setting up the TPS model and, in the case of Isomap, the computation of the proper number of nearest neighbors [15]. Although there is a big difference between the building times of Isomap+I and POD+I, compared to a full CFD calculation the offline times (without the snapshot computations) are negligible. The online prediction of a surface solution at an untried parameter combination $\tilde{\mathbf{p}} \in \mathcal{P} \setminus P$ took less than 0.01 CPU seconds for both ROMs, whereas a full CFD solution took 4214 CPU seconds on average. In other words, the predictions of both ROMs are more than 400,000 times faster than a full CFD solution, but certainly due to a trade-off of less accuracy.

---

[4]The mean of the snapshots is subtracted.

Table 3 Errors in terms of equation (1) between the TAU reference surface C_p solutions and the surface C_p predictions obtained by Isomap+I, Isomap+LSQ, POD+I and POD+LSQ at various parameter combinations. The column NN lists the number of nearest neighbors employed by the Isomap based predictions at each parameter combination $\tilde{\mathbf{p}}$.

$\tilde{\mathbf{p}}$	NN	Isomap+I	Isomap+LSQ	POD+I	POD+LSQ
1	11	$8.5930 \cdot 10^{-2}$	$7.1702 \cdot 10^{-2}$	$9.4556 \cdot 10^{-2}$	$5.9426 \cdot 10^{-2}$
2	16	$8.7347 \cdot 10^{-2}$	$7.5275 \cdot 10^{-2}$	$1.1523 \cdot 10^{-1}$	$5.5323 \cdot 10^{-2}$
3	14	$7.7126 \cdot 10^{-2}$	$7.5143 \cdot 10^{-2}$	$9.4977 \cdot 10^{-2}$	$6.3302 \cdot 10^{-2}$
4	10	$1.0089 \cdot 10^{-1}$	$1.3703 \cdot 10^{-1}$	$1.3514 \cdot 10^{-1}$	$6.4285 \cdot 10^{-2}$
5	20	$6.4210 \cdot 10^{-2}$	$7.1029 \cdot 10^{-2}$	$7.7599 \cdot 10^{-2}$	$5.7465 \cdot 10^{-2}$
6	10	$7.0431 \cdot 10^{-2}$	$9.3372 \cdot 10^{-2}$	$7.7246 \cdot 10^{-2}$	$5.9561 \cdot 10^{-2}$
7	14	$6.7638 \cdot 10^{-2}$	$5.1527 \cdot 10^{-2}$	$9.1839 \cdot 10^{-2}$	$4.4243 \cdot 10^{-2}$
8	10	$4.3445 \cdot 10^{-2}$	$4.5011 \cdot 10^{-2}$	$8.9193 \cdot 10^{-2}$	$3.0280 \cdot 10^{-2}$
9	13	$5.6208 \cdot 10^{-2}$	$4.0005 \cdot 10^{-2}$	$7.4482 \cdot 10^{-2}$	$2.8970 \cdot 10^{-2}$
10	10	$6.3993 \cdot 10^{-2}$	$5.9396 \cdot 10^{-2}$	$8.7417 \cdot 10^{-2}$	$4.1372 \cdot 10^{-2}$

The resulting surface C_p-distributions predicted by Isomap+I and POD+I for various parameter combinations are compared to the corresponding TAU reference solutions. The corresponding errors in terms of equation (1) for the predictions points are given in Table 3. The Isomap+I predictions feature a smaller error than the POD+I predictions. An example of the ROM aerodynamic loads predictions (in terms of surface C_p-distribution) for an untried parameter combination ($\tilde{\mathbf{p}}^8$ of Table 3) is given in Fig. 13. The Isomap+I prediction matches the surface C_p-distribution of the TAU reference solution quiet accurately. The POD+I prediction also yields accurate predictions, but the C_p-distribution between the first two sections differs from the reference solution.

Of course, due to the complexity of the test case, where arbitrary twists at the five sections of the wing are analysed, there could be cases where the ROM predictions are less accurate, so leading to bigger errors (see e.g. the parameter combination $\tilde{\mathbf{p}}^4$ in Table 3).

The spanwise distributions of the partial force f_z and the partial moment m_y, calculated via AeroForce [41], are shown for the parameter combination $\tilde{\mathbf{p}}^8$ in Fig. 14. As it can be seen, there is a good match between the force and moment distributions of the reference solution and those of the ROM prediction.

3.3.2 Isomap with Residual Optimization

The interpolation-based Isomap and POD coefficients can be then exploited as starting values for the residual based ROM [15]. The unconstrained optimization problems are solved now. To optimize the coefficients of an Isomap or POD based prediction, the Levenberg-Marquardt algorithm [29, 42] with additional Broy-
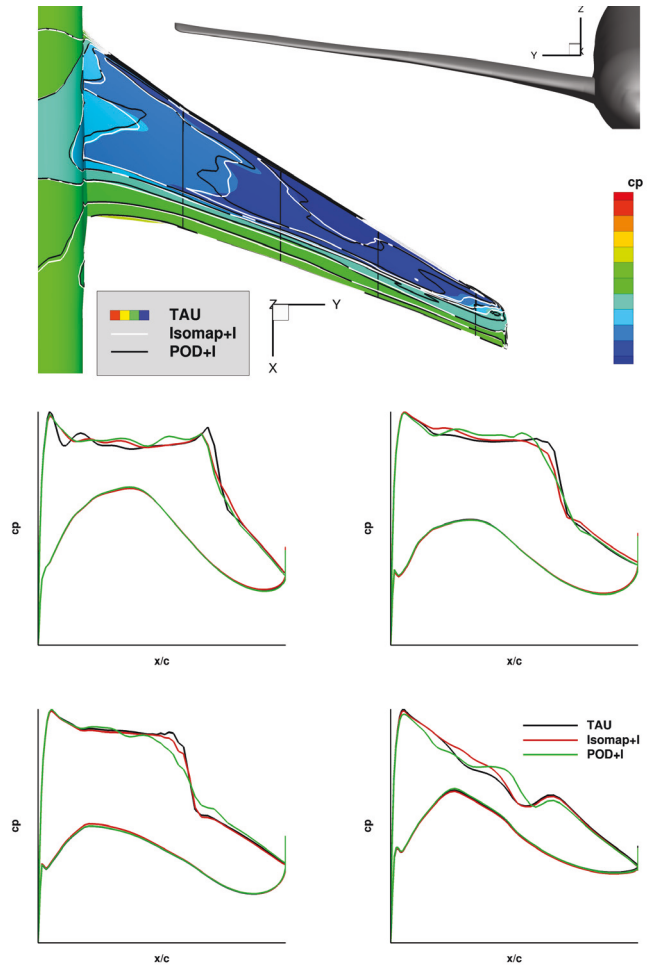

Fig. 13 Prediction of the surface C_p-distribution of the XRF-1 by Isomap+I and POD+I at an untried parameter combination $\tilde{\mathbf{p}}^8 \in \mathcal{P} \setminus P$. The four section cuts, ordered line by line from left to right, correspond to the twist sections from fuselage to tip.

den's rank one updates of the Jacobian is applied to the unconstrained optimization problems [15].

All primitive variables plus the C_p-distribution are taken into account, leading to a set of snapshots $W \subset \mathbb{R}^n$, $n = n_g \cdot n_v = 6,275,072$. Hence, Isomap+LSQ and POD+LSQ are based on 100 snapshots of dimension $n = 6,275,072$, increasing the building time of the POD based ROM to 117 CPU seconds. The costs of Isomap+LSQ (119 CPU seconds) remains unaffected of the new data set, as only the surface C_p-distribution is exploited to compute the embedding.

The residual has to be evaluated with proper boundary conditions Ma and α, which are not specified by the varied parameters. While the Mach number Ma is fixed, the angle of attack α varies for each flow solutions to ensure the specified target C_l value. Here, the
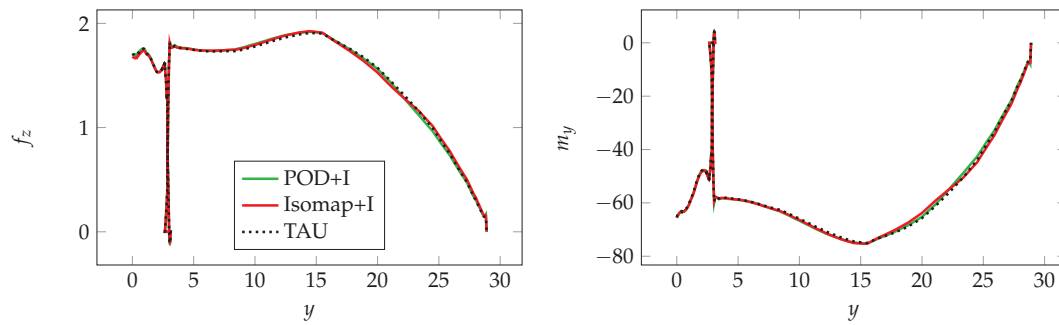
Fig. 14 Spanwise distributions of the force f_z and moment m_y at the $\tilde{\mathbf{p}}^8$ predictions point.

angle of attack α is obtained from the corresponding reference solution to exclude additional error sources which would affect the accuracy of the C_p predictions. After evaluating the TAU residual, the discrepancy in the total energy values belonging to the 20% smallest cells is exploited by the objective function to optimize the coefficient vector $\mathbf{a} \in \mathbb{R}^d$, until the tolerance of termination ($tol = 1.49012 \cdot 10^{-8}$) is reached.

The CFD enhanced predictions obtained throught the residual optimization have been computed for different untried parameter combinations [15]. It can be seen (Table 3) that the corresponding errors in terms of equation (1) of both ROMs (Isomap+LSQ and POD+LSQ) are reduced.

Unlike the POD+LSQ, the application of the residual optimization to Isomap (Isomap+LSQ) increases the error at few parameter combinations $\tilde{\mathbf{p}}$ for this set up. However, an improvement of the predictions is observed in most cases. Comparing the CPU times in Table 4, due to the less DoF the Isomap+LSQ predictions are up to 4 times faster than the POD+LSQ predictions and, in average, 7.5 times faster than a full CFD computation.

3.4 Reduced-Order Models for Aerodynamic Loads and Structural Sizing

In the context of MDO a CFD solver is repeatedly used to perform fluid/structure-coupled simulations. Typically, the entire optimization process consists of two nested loops: an inner loop, where different load cases are computed to size the different optimization regions of the structural model for a given aerodynamic shape, and an outer loop where performance data is computed and used to optimize the shape of the wing or aircraft according to some objective function. Since the computations of the full-order CFD solutions are expensive and repeatedly required in both loops, ROM may provide remedy. For the outer loop, the

Table 4 Number of iterations and CPU times of conducting Isomap+LSQ and POD+LSQ predictions for the XRF-1 test case. The gained speed-up by performing Isomap+LSQ instead of POD+LSQ is stated in the last column.

	Isomap+LSQ		POD+LSQ		speed-up
$\tilde{\mathbf{p}}$	iter	CPU times (s)	iter	CPU times (s)	factor
1	23	568.39	19	1,905.21	3.35
2	27	714.16	19	1,900.94	2.66
3	19	557.12	17	1,873.29	3.36
4	22	540.33	19	1,905.38	3.53
5	21	682.94	21	1,920.56	2.81
6	18	479.97	19	1,904.7	3.97
7	19	554.35	14	1,816.53	3.28
8	22	539.72	19	1,897.45	3.52
9	18	523.81	16	1,849.99	3.53
10	18	480.95	15	1,829.26	3.8

steady aerodynamic ROM introduced in Section 3.3.1 and Section 3.3.2 can be exploited to compute the necessary aerodynamic quantities for the optimization of the geometry, since the variation of the geometry is taken into account. The advantage of substituting the CFD solver with a ROM is that the snapshots and the ROM are computed offline before the optimization takes place. This should lead to a speed-up of the actual optimization process or rather to a larger amount of load cases that can be considered for the structural sizing in the inner loop.

To demonstrate the idea it is assumed here that the aircraft is rigid, i.e., there is no need to perform fluid/structure-coupled simulations. This is true for some very stiff models, e.g., for wind-tunnel models. A rigid aircraft may also be assumed when computing CFD-based corrections to a linear potential flow solution in the context of loads computations (so-called AIC corrections). Furthermore, a single (steady) load case is here used to size the structural model. Hence, skipping the inner loop, the ROM for the XRF-1 are exploited to predict the steady surface C_p-distributions
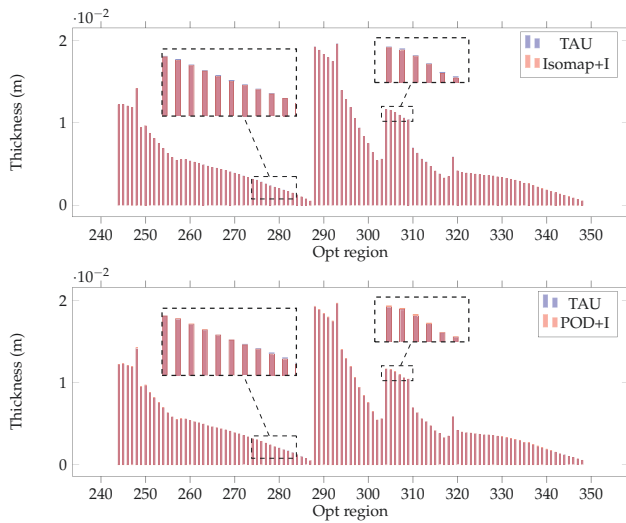
Fig. 15 Thicknesses at the wing spar optimization regions for the predictions of Isomap+I (top) and POD+I (bottom) at $\mathbf{p}^3$. Emphasized are the regions with largest gap.

for different geometries, which afterwards are fed into the structural sizing process to obtain the skin thickness of each optimization region.

For the XRF-1 test case, the structural optimization regions are divided into upper skin regions, lower skin regions, wing ribs regions and wing spar regions. The skin thicknesses at the wing spar, which is the main structural member of the wing, are shown in Fig. 15 for the $\tilde{\mathbf{p}}^3$ predictions point. The three spars are divided in the optimization regions from 234 to 287, 288 to 303 and 304 to 347. Since there are three wing spars, the thickness distribution plotted against the optimization region does not show a decreasing behaviour as usual, but for each separate spar it does. However, close to the optimization region 320, there is an outlier which may be due to the fact that the inner spar, with corresponding optimization regions 288 to 303, ends and the loads are distributed to the two remaining spars. As it can be seen, Isomap and POD-based ROM provide good predictions of the thickness distributions at the wing spar optimization regions. Particularly, the detailed views emphasize that there is almost no mismatch between the computed thicknesses of the predicted solutions and the computed thicknesses of the corresponding reference solutions. Thus, these ROM are suitable in the context of MDO and should lead to a speed-up of the optimization process as mentioned above.

4 Reduced Order Models of Aerodynamic Influence Coefficients

In the context of the MDO process in the Digital-X project, loads analysis plays a central role [25]. It is responsible for determining the loads envelope of the current design iteration and size the structure to comply with structural limits on the so called "Dynamic level" (ref. Fig. 1), before higher fidelity methods are applied to make a detailed analysis of the intermediate result.
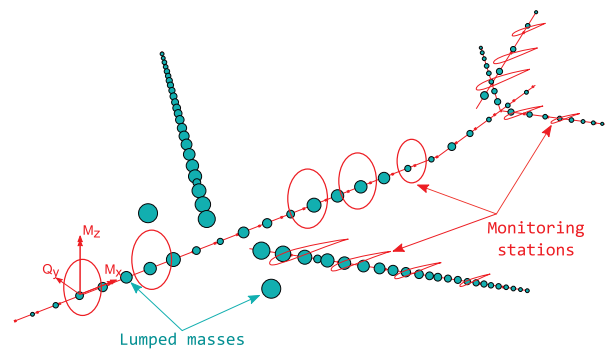
(a) Internal loads submodels
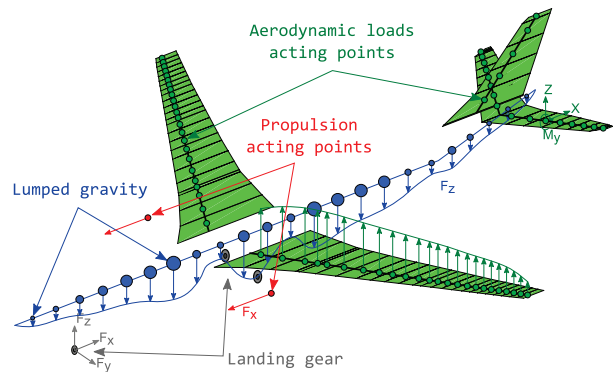
(b) External loads submodels

Fig. 16 Schematic loads submodels for a generic 2-engine passenger aircraft.

4.1 Loads Analysis

Loads analysis on the dynamic level takes into account a large amount of load cases in accordance with FAR §25 requirements covering trim cases, dynamic maneuvers and gust encounters across the flight envelope. To get results in a reasonable amount of time,

this automated process has to be as fast as possible. To this end several simplifications are applied during model integration, the result of which is represented schematically in Fig. 16.

- The process starts out with a full Finite Element (FE) structural model containing some 72000 DoF, this model is condensed onto componentwise loads reference axes (LRA) using a Guyan reduction, yielding 3000 DoF. Subsequent modal analysis reduces the structural DoF further to e.g. 40.
- The same Guyan transformation is also used to condense the structural mass distribution to the nodes on the loads reference axes. Fuel and secondary masses are then attached to these nodes to form a lumped mass model.
- The aerodynamic governing equations are the Prandtl-Glauert potential flow equations. They may be used either in their unsteady or in their steady Laplace form, depending on the load case requirements. These linear equations are discretized on a mean lifting surface grid instead of throughout the volume around the aircraft, thereby dramatically reducing the number of elements required to solve for the surface pressure distribution. For unsteady cases, the discretization uses doublet elements to model the lifting effect of each panel, yielding the Doublet Lattice Method (DLM). Steady flows are discretized using horseshoe-shaped vortex elements, yielding the Vortex Lattice Method (VLM). Solving the problem for a grid with many elements, including the interactions of elementary flows among the panel control points, leads to the Aerodynamic Influence Coefficient (AIC) matrix. The AIC relates pressure differences at the panel control points to the downwash velocities at the panel 3/4-chord points. VLM yields a real-valued AIC, while DLM produces a complex-valued AIC matrix.
  As both VLM and DLM use the same panel grid, they may be combined to solve unsteady flow problems with a steady component. DLM is solved in the frequency domain, whereas VLM is directly applicable to quasi-steady time domain problems. To obtain transient time domain solutions an inverse Laplace transformation is applied to the frequency domain solution via a Rational Function Approximation (RFA).

These submodels are then integrated by connecting the structural LRA nodes to the aerodynamic panel control point set using a splining scheme. This yields a fast and iteration-free coupling between structure and aerodynamic models.

The Prandtl-Glauert equations governing the aerodynamic part of the loads model may be traced back from the Navier Stokes equations through a number of simplifying assumptions, as summarized in Table 5. To overcome the absence of non-linear flow phenom-

Table 5 Some flow governing equations and corr. assumptions which accumulate downward.

Assumption	Equation	effect neglected
continuum fluid mechanics	Navier Stokes	no molecular dynamics
inviscid	Euler	boundary layer, turbulence
irrotational, isentropic	Full Potential	no strong shocks
small disturbances	transonic small disturb. (TSD)	no blunt bodies
linearized	Prandtl-Glauert	no transonic effects
time-independent	Laplace	no unsteady effects

ena, several AIC correction methods have been developed. These reintroduce the effects at specific flight conditions by comparing with corresponding higher fidelity results. Giesing et al.[17] propose a diagonal multiplicative technique, which was extended to a full correction factor matrix by Jadic et al.[21]. Brink-Spalink et al.[8] describe an additive AIC correction technique based on weighted least squares optimization. In general, these methods may use either empirical data or higher fidelity computational flow results as a basis for correction.

Here, we present the combination of an additive AIC correction method with the concept of the ROM through proper orthogonal decomposition of the AIC matrices rather than the pressure distributions themselves. This has the advantage of retaining the integrated loads model and fast simulation capability as described earlier, while also introducing the non-linear effects of high fidelity CFD solutions.

Moreover, by coupling the AIC-ROM to a multi-dimensional spline interpolation method, we can evaluate at any parameter combination within the domain of correction *and have a flow parameter-complete aerodynamics model* in a neighborhood around the correction point due to the linear nature of VLM. The AIC matrix relates local differential pressures to local downwash, or equivalently, angle of attack. Every global flow parameter (except Mach) is translated to a contribution to the downwash distribution on the lifting surface panel grid. This means that we may correct for the principal higher order flow phenomena associated with varying Mach number and angle of attack and use the resulting model with load cases which require non-zero rotational rates, control surface deflections and bending modes while still benefiting from the correction.
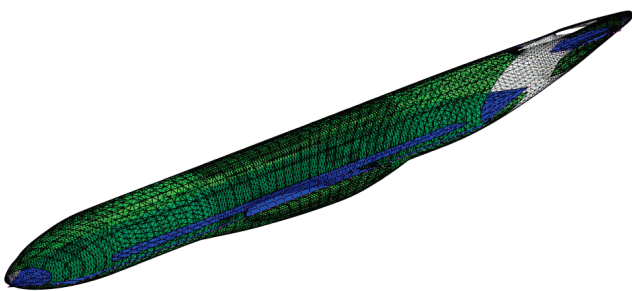
4.2 Surface Geometry Mapping

Since the source for correction of the VLM model in this work are surface pressure distributions from CFD solutions, the correction process must start with a geometric mapping from the CFD mesh onto the VLM panel grid.

The objective is to have an equivalent VLM pressure distribution which is accurate both globally and locally when comparing cross-sections.

There are significant geometry restrictions associated with the VLM method. Specifically, VLM being a lifting surface method, it discretizes the mean surface of aerodynamic components producing a model without internal volume. Also, individual panels are not allowed incidence angles to the nominal oncoming flow direction (usually equivalent to $\alpha = 0°, \beta = 0°$). Instead, the VLM pressure distribution results from circulation induced by linearized small incidence angles. These restrictions mean that there are considerable geometric differences to overcome in the mapping process. An overview follows with an example illustrating
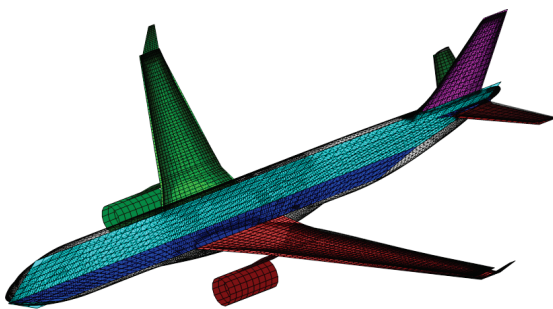
(a) CFD mesh and VLM panel grid overlay

(b) perpendicular mapping of the horizontal fuselage panels

Fig. 17 Component-wise geometry mapping.

the procedure shown in Fig. 17:

- The global coordinate frames of both geometries are related to one another through a translation and a rotation, in order to optimize the match. A

visual inspection may be necessary at this point to uncover potential mismatches in e.g. component planforms, dihedral, etc. as these may necessitate correction of the VLM model geometry. It may happen that some components are missing in the CFD geometry. Such is the case in Fig. 17(a) with the engines and winglets. As mapping proceeds component-wise however, these components may simply be left out at this point. Later these uncorrected components will be present in the corrected model and still provide interaction effects with the corrected components.

- Assuming a planar component such as a wing or tail surface, there will be two opposing surfaces in the CFD geometry to be mapped onto the single surface of the component's VLM representation. This means the result will be a pressure difference. The method proceeds by cutting the CFD geometry perpendicular to each VLM panel. This includes cutting individual faces and interpolating pressure values at the newly created nodes as shown in Fig. 17(b).
- The selected areas and their pressure values have to be related to the load control point of the associated panel. First, force vectors are calculated for each CFD element.
- These forces are then integrated onto the panel load control point using a rigid splining scheme.
- The three matrix operations may be combined to yield a single mapping matrix, which may be concatenated for all panels in the component. Thus, the mapping process may be conveniently stored as a small collection of mapping matrices corresponding to the aircraft components included in the process.
- In the case of planar components like wings and tailplanes the above suffices. However tubelike components such as the fuselage in Fig. 17 may be modelled by two perpendicular planes for the VLM method. In this case the mapping process needs a refinement: The CFD loads are decomposed vector-wise and the y- and z-components are projected onto the perpendicular planes. The x-component is distributed using the ratio of distances to both planes. This decomposition conserves integrated loads as well as the spanwise distributions.

4.3 AIC correction

At its core, simulation using the VLM method involves solving

$$C_{p_j} = Q_{jj}D_{jx}U_x, \tag{2}$$

where $Q_{jj} \in \mathbb{R}^{n \times n}$ is the AIC matrix for an n-panel grid, $D_{jx} \in \mathbb{R}^{n \times k}$ is the downwash matrix and $U_x \in \mathbb{R}^{k \times 1}$ is the flight state parameter vector, e.g. containing free-stream flow angles, rotational rates, control surface deflections and modal coordinates of bending modes.

In order to correct the VLM model, the AIC matrix has to be adapted to the mapped CFD loads distribution. However, as Q_{jj} is responsible for the gradient of the pressure distribution, changing it will generally also result in a non-zero pressure offset vector $C_{p_0} \in \mathbb{R}^n$.

To solve the AIC matrix correction, the VLM gradient (denoted by $^{(v)}$)

$$G_{jx}^{(v)} := Q_{jj}^{(v)} D_{jx} \tag{3}$$

may be equated to the CFD gradient $G_{jx}^{(c)}$ (denoted by $^{(c)}$) and solved for the corrected AIC matrix Q_{jj}^* through Kronecker product vectorization:

$$\text{vec } G_{jx}^{(c)} = \left(D_{jx}^T \otimes I_n \right) \text{vec } Q_{jj}^*, \tag{4}$$

where I_n is the n-dimensional identity matrix.
This under-determined problem has a nonempty set of solutions provided that $D_{jx}^T \otimes I_n$ has full rank. One particular solution is the least norm solution, minimizing $\| \text{vec } Q_{jj}^* \|$ using a pseudo inverse [31] (denoted as $(\cdot)^\dagger$).
However, since the VLM AIC $Q_{jj}^{(v)}$ provides a baseline solution, a more physically meaningful approach would be to minimize the norm of the difference $\Delta Q_{jj} = Q_{jj}^{(v)} - Q_{jj}^*$ as it minimizes the changes applied to $Q_{jj}^{(v)}$. This may be achieved as follows:

$$\Delta G_{jx} = \Delta Q_{jj} D_{jx} \quad \Rightarrow \tag{5}$$

$$\text{vec } \Delta G_{jx} = \left(D_{jx}^T \otimes I_n \right) \text{vec } \Delta Q_{jj} \quad \Rightarrow$$

$$\text{vec } \Delta Q_{jj} = \left(D_{jx}^T \otimes I_n \right)^\dagger \text{vec } \Delta G_{jx} \tag{6}$$

$$Q_{jj}^* = Q_{jj}^{(v)} - \Delta Q_{jj}$$

For problems with 1000s of panels ($n > 1000$), solving Eq. (6) directly becomes inefficient even with sparse data types. However, Eq. (6) lends itself well to a row-wise computation which alleviates a computer's memory capacity problems and enables the solving of arbitrarily large problems. Furthermore, breaking the problem up into pieces consisting of a number of rows allows for speed optimization.

After the desired Q_{jj}^* has been solved for, the pressure offset vector may be found by taking the surface pressure vector from CFD $C_p^{(c)}$ and solving

$$C_{p_0} = C_p^{(c)} - Q_{jj}^* D_{jx} U_x \tag{7}$$

To determine the CFD gradient, we use a simple forward difference quotient to limit the number of required CFD solutions:

$$G_{jx_i}^{(c)} = \frac{\partial C_p(U_x)}{\partial U_{x_i}} \approx \frac{C_p(U_{x_i} + h_i) - C_p(U_{x_i})}{h_i},$$

where the subscript i denotes the global flow parameter in U_x and $G_{jx_i}^{(c)}$ is the corresponding column of the gradient matrix $G_{jx}^{(c)}$. The AIC matrix may be corrected with respect to a subset of U_x by including only the corresponding columns of the downwash matrix D_{jx} in Eq. (5).

4.4 POD Interpolation

The first step is to build the snapshot matrix Y for both the ensemble of AICs and offsets. This is done by concatenating the vectorized AIC matrices on the one hand and concatenating the pressure offset vectors directly on the other hand.

The resulting POD for either case may be written compactly as $Y^T Y V = V \Lambda$, where $V = [v_1, \ldots v_l]$ is an $n \times l$ matrix composed of eigenvectors and $\Lambda = \text{diag}(\lambda_1, \ldots, \lambda_l)$ is an $l \times l$ diagonal matrix with the corresponding eigenvalues.

To facilitate interpolation, the POD is formulated as the product of two quantities: $\Phi = Y \cdot V \in \mathbb{R}^{m \times l}$ and $H = V^T \in \mathbb{R}^{l \times n}$ such that, if l is chosen equal to d, we obtain $Y = \Phi \cdot H$ and for a smaller number of retained eigenvectors $\Phi \cdot H$ approximates Y optimally given the choice of l. The columns of $H = [\eta_1, \ldots \eta_n]$ may be interpreted as the modal coordinates of the POD. Each η_i for $i = 1, \ldots, n$ corresponds to a corrected flight state with parameter vector $x_i \in X$.

A multivariate interpolation method may now be used to map H onto X giving η as a function of any desired flight condition x^*. The Thin Plate Spline (TPS), a form of Radial Basis Function (RBF) spline, is here used. It is well-behaved and has only one free parameter. Beckert and Wendland [6] describe the TPS and a number of alternatives in a fluid dynamics context.

Finally, to obtain the corrected AIC matrix and pressure offset at x^*, we apply the results from the

interpolation method $\eta(x^*)$ to the POD data matrix Φ:

$$y(x^*) \approx \Phi \cdot \eta(x^*) \rightarrow$$
$$\text{vec}\, Q_{jj}(x^*) \approx \Phi_{Q_{jj}} \cdot \eta_{Q_{jj}}(x^*)$$
$$C_{p_0}(x^*) \approx \Phi_{C_{p_0}} \cdot \eta_{C_{p_0}}(x^*)$$

4.5 Results

Figure 18 illustrates the presented AIC-ROM method. The figure shows aerodynamic distributions on a wing subjected to a steady roll rate. The VLM model has been corrected at several (M, α) combinations, but not for nonzero roll rates. This corrected model is then assembled into POD and interpolated at the flight state indicated by the red diamond in Fig. 18(a). The roll rate is applied to the AIC matrix in the same manner as with the uncorrected VLM model. Finally, both corrected and uncorrected models have been compared to a new CFD solution. The figure shows that the (M, α) correction is also valid at asymmetric flight states with e.g. large roll rates.

5 Summary

The effectiveness of parametric CFD-based, linear and nonlinear, reduced order models have been demonstrated in the context of an MDO process.

Static aeroelastic loads of the XRF1 aircraft are predicted at different flight conditions with a a good level of accuracy for aircraft design purposes, and a great speed-up compared to a high-fidelity full-order fluid/structure coupled simulation. The accuracy and low computational cost of the ROM loads prediction allows an improved selection of the critical loads, by rapidly spanning the flight envelope parameter space. This provides additional critical load cases which would otherwise not be found by the high-fidelity only approach. The ROM-predicted aerodynamic loads are then shown to be accurate enough to be used for structural sizing, leading to results comparable to high-fidelity methods, but with a great reduction of the computational time.

The AIC-ROM method has been introduced. Its role in "dynamic level" loads analysis and sizing process is to provide improved aerodynamic fidelity by reintroducing complex flow phenomena which are absent in the fast potential flow methods used in this process. We have shown its ability to replicate flow states for roll rates when this parameter is absent in the snapshot dataset. This is due to the AIC-ROM's inherent parameter-completeness.
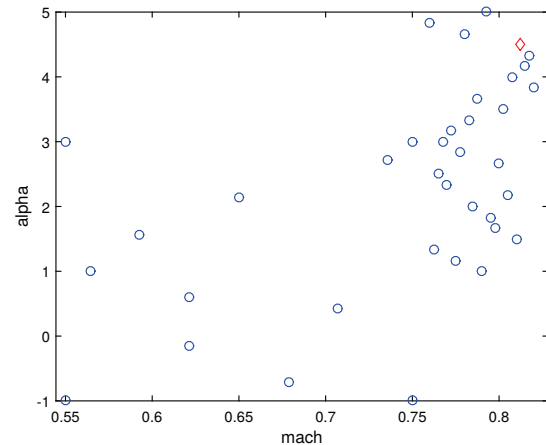
(a)
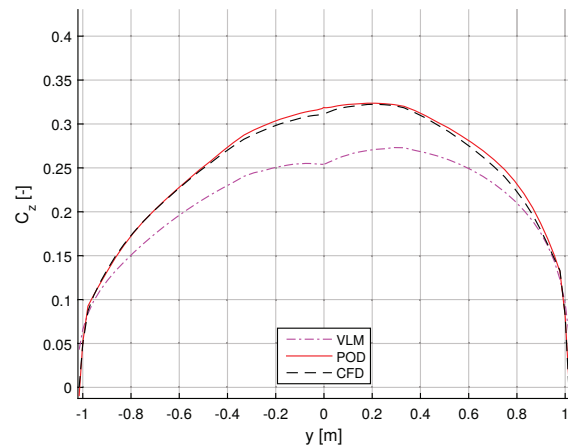
(b)
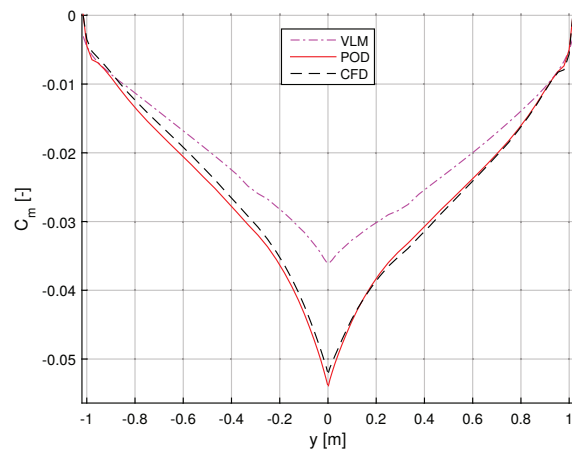
(c)

Fig. 18 Demonstration of the AIC-ROM method using a steady roll rate applied to the LANN wing. The CFD solution points used for the correction vary only in M and α as shown in subfigure a. The corrected model is then subjected to a large roll rate and the resulting spanwise C_Z and C_m distributions are compared to a new CFD solution in subfigures b & c, respectively. VLM denotes the original model, POD the corrected model and CFD the reference solution.

References

1. Allmaras, S.R., Johnson, F.T.: Modifications and clarifications for the implementation of the spalart-allmaras turbulence model. In: Seventh International Conference on Computational Fluid Dynamics (ICCFD7), pp. 1–11 (2012)

2. Astrid, P.: Reduction of process simulation models: a proper orthogonal decomposition approach. Ph.D. thesis, Technische Universiteit Eindhoven (2004)

3. Astrid, P., Weiland, S., Willcox, K., Backx, T.: Missing point estimation in models described by proper orthogonal decomposition. Automatic Control, IEEE Transactions on **53**(10), 2237–2251 (2008)

4. Barber, C.B., Dobkin, D.P., Huhdanpaa, H.: The quickhull algorithm for convex hulls. ACM Transactions on Mathematical Software (TOMS) **22**(4), 469–483 (1996)

5. Barrault, M., Maday, Y., Nguyen, N.C., Patera, A.T.: An 'empirical interpolation'method: application to efficient reduced-basis discretization of partial differential equations. Comptes Rendus Mathematique **339**(9), 667–672 (2004)

6. Beckert, A., Wendland, H.: Multivariate interpolation for fluid-structure-interaction problems using radial basis functions. Aerospace Science and Technology **5**(2), 125–134 (2001). DOI 10.1016/S1270-9638(00)01087-7

7. Bernstein, A.V., Kuleshov, A.P.: Tangent bundle manifold learning via grassmann & stiefel eigenmaps. CoRR **abs/1212.6031** (2012)

8. Brink-Spalink, J., Bruns, J.M.: Correction of Unsteady Aerodynamic Influence Coefficients using Experimental or CFD Data. In: International Forum on Aeroelasticity and Structural Dynamics (2001)

9. Bui-Thanh, T., Damodaran, M., Willcox, K.: Proper orthogonal decomposition extensions for parametric applications in transonic aerodynamics. In: Proceedings of the 21th AIAA Applied Aerodynamics Conference. AIAA, Orlando, Florida (2003). DOI 10.2514/6.2003-4213

10. Cayton, L.: Algorithms for manifold learning. Univ. of California at San Diego Tech. Rep pp. 1–17 (2005)

11. Chaturantabut, S., Sorensen, D.C.: Nonlinear model reduction via discrete empirical interpolation. SIAM Journal on Scientific Computing **32**(5), 2737–2764 (2010)

12. Forrester, A., Sóbester, A., Keane, A.: Engineering design via surrogate modelling: a practical guide. John Wiley & Sons (2008)

13. Fossati, M.: Evaluation of Aerodynamic Loads via Reduced-Order Methodology. AIAA Journal (2015)

14. Fossati, M., Habashi, W.G.: Multiparameter analysis of aero-icing problems using proper orthogonal decomposition and multidimensional interpolation. AIAA journal **51**(4), 946–960 (2013)

15. Franz, T.: Reduced-order modeling for steady transonic flows via manifold learning. Ph.D. thesis, TU Braunschweig (2016). URL http://www.digibib.tu-bs.de/?docid=00062584

16. Franz, T., Zimmermann, R., Görtz, S., Karcher, N.: Interpolation-based reduced-order modelling for steady transonic flows via manifold learning. International Journal of Computational Fluid Dynamics **28**(3–4), 106–121 (2014)

17. Giesing, J.P., Kalman, T.P., Rodden, W.P.: Correction Factor Techniques for Improving Aerodynamic Prediction Methods. Tech. rep., NASA (1976)

18. Görtz, S., Ilić, v., Liepelt, R.: Collaborative Multilevel MDO Process Development and Application to Long-ranged Transport Aircraft. In: ICAS (2016)

19. Hofstee, J., Kier, T., Cerulli, C., Looye, G.: A Variable, Fully Flexible Dynamic Response Tool for Special Investigations (VarLoads). In: Proceedings of the International Forum on Aeroelasticity and Structural Dynamics (IFASD). Amsterdam, The Netherlands (2003)

20. Holmes, P., Lumley, J.L., Gahl Berkooz, Rowley, C.W.: Turbulence, Coherent Structures, Dynamical Systems and Symmetry, first edn. Cambridge University Press (1996). ISBN 978-0-521-55142-7

21. Jadic, I., Hartley, D., Giri, J.: An Enhanced Correction Factor Technique for Aerodynamic Influence Coefficient Methods. In: MSC Aerospace User's Conference (1999)

22. Kroll, N., Abu-Zurayk, M., Dimitrov, D., Franz, T., Führer, T., Gerhold, T., Görtz, S., Heinrich, R., Ilic, C., Jepsen, J., Jägersküpper, J., Kruse, M., Krumbein, A., Langer, S., Liu, D., Liepelt, R., Reimer, L., Ritter, M., Schwöppe, A., Scherer, J., Spiering, F., Thormann, R., Togiti, V., Vollmer, D., Wendisch, J.H.: Dlr project digital-x: Towards virtual aircraft design and flight testing based on high-fidelity methods. CEAS Aeronautical Journal **7**(1), 3–27 (2016)

23. Langer, S., Schwöppe, A., Kroll, N.: The DLR flow solver TAU-status and recent algorithmic developments. In: 52nd AIAA Aerospace Sciences Meeting. AIAA Paper, vol. 80 (2014)

24. LeGresley, P.A., Alonso, J.J.: Investigation of Non-Linear Projection for POD Based Reduced Order Models for Aerodynamics. In: Proceedings of the 39th AIAA Aerospace Sciences Meeting and Exhibit, vol. 926, p. 2001. Reno, Nevada (2001)

25. Leitner, M., Liepelt, R., Kier, T., Klimmek, T., Müller, R., Schulze, M.: A Fully Automatic Structural Optimization Framework to Determine Critical Design Loads. In: Deutscher Luft- und Raumfahrt Kongress 2016. Braunschweig, Germany (2016)

26. Lucia, D.J., Beran, P.S., Silva, W.A.: Reduced-order modeling: new approaches for computational physics. Progress in Aerospace Sciences **40**(1), 51–117 (2004)

27. Van der Maaten, L., Postma, E., Van den Herik, H.: Dimensionality reduction: A comparative review. Journal of Machine Learning Research **10**, 1–41 (2009)

28. Mardia, K., Kent, J., Bibby, J.: Multivariate analysis. Academic press (1979)

29. Moré, J.J.: The levenberg-marquardt algorithm: implementation and theory. In: Numerical analysis, pp. 105–116. Springer (1978)

30. Narayanan, H., Mitter, S.: Sample complexity of testing the manifold hypothesis. In: Advances in Neural Information Processing Systems, pp. 1786–1794 (2010)

31. Penrose, R.: On best approximate solutions of linear matrix equations. Mathematical Proceedings of the Cambridge Philosophical Society **52**(1), 17–19 (1956)

32. Piperni, P., DeBlois, A., Henderson, R.: Development of a multilevel multidisciplinary-optimization capability for an industrial environment. AIAA Journal **51**, 2335–2352 (2013). DOI 10.2514/1.J052180

33. Rajan, V.: Optimality of the delaunay triangulation in $\mathbb{R}^d$. Discrete & Computational Geometry **12**(1), 189–202 (1994)

34. Schilders, W.H., Van Der Vorst, H.A., Rommes, J.: Model order reduction: theory, research aspects and applications, vol. 13. Springer (2008)

35. Schwamborn, D., Gerhold, T., Heinrich, R.: The DLR TAU-code: recent applications in research and industry, tech. report. In: European Conference on Computational Fluid Dynamics, ECCOMAS CFD 2006. Egmond and Zee, The Netherlands (2006)

36. Shlens, J.: A tutorial on principal component analysis. Systems Neurobiology Laboratory, University of California at San Diego (2005)

37. Tenenbaum, J.B., de Silva, V., Langford, J.C.: A Global Geometric Framework for Nonlinear Dimensionality Reduction. Science **290**(5500), 2319–2323 (2000)

38. Tropea, C., Yarin, A., Foss, J.: Springer Handbook of Experimental Fluid Mechanics. Springer-Verlag Berlin Heidelberg (2007)

39. Vendl, A., Faßbender, H.: Model order reduction for unsteady aerodynamic applications. In: Proc. Appl. Math. Mech., vol. 13, pp. 475–476 (2013)

40. Vendl, A., Faßbender, H., Görtz, S., Zimmermann, R., Mifsud, M.: Model order reduction for steady aerodynamics of high-lift configurations. CEAS Aeronautical Journal **5**(4), 487–500 (2014)

41. Wild, J.: Aeroforce - thrust/drag bookkeeping and aerodynamic force breakdown over components. Tech. rep., German Aerospace Center (DLR) (1999)

42. Wright, S., Nocedal, J.: Numerical optimization, vol. 2. Springer New York (1999)

43. Zill, T., Böhnke, D., Nagel, B.: Preliminary Aircraft Design in a Collaborative Multidisciplinary Design Environment. In: AIAA Aviation Technology, Integration and Operations (2011)

44. Zimmermann, R., Görtz, S.: Non linear reduced order models for steady aerodynamics. In: Procedia Computer Science, vol. 1, pp. 165–174 (2010). Proceedings of the International Conference on Computational Science, ICCS 2010

45. Zimmermann, R., Görtz, S.: Improved extrapolation of steady turbulent aerodynamics using a non-linear POD-based reduced order model. The Aeronautical Journal **116**(1184), 1079–1100 (2012)

46. Zimmermann, R., Vendl, A., Görtz, S.: Reduced-order modeling of steady flows subject to aerodynamic constraints. AIAA Journal pp. 1–12 (2014)

47. Zimmermann, R., Willcox, K.: An accelerated greedy missing point estimation procedure. SIAM Journal on Scientific Computing (2016). Accepted for publication